ELSEVIER

Journal of Nuclear Materials 307–311 (2002) 783–787

journal of nuclear materials

www.elsevier.com/locate/jnucmat

Structure, radiation resistance and thermal creep of ODS ferritic steels

B.N. Goshchitskii [a,*], V.V. Sagaradze [a], V.I. Shalaev [a], V.L. Arbuzov [a], Yun Tian [b], Wan Qun [c], Sun Jiguang [c]

[a] *Institute of Metal Physics, UB RAS, S. Kovalevskoii Str. 18, Ekaterinburg GSP-170 620219, Russia*
[b] *Central Iron and Steel Research Institute, Beijing 100081, China*
[c] *General Research Institute for Non-ferrous Metals, Beijing 100088, China*

Abstract

The microstructure, tensile properties and high-temperature creep of oxide dispersion strengthened (ODS) ferritic steels were investigated. It was shown that a high degree of hardening of ODS steels is determined by a large density of dislocations and dispersed yttrium oxides 2–3 nm in diameter. ODS steels have significant advantages over typical ferritic–martensitic steels with respect to their creep resistance and strength under high stress and temperature. The kinetics of accumulation and annealing of radiation defects under electron and neutron irradiation at 77 and 340 K, and the effect of neutron irradiation at 77 and 683 K on tensile properties of ODS steels were studied.

1. Introduction

Recently we have seen the advent of ferritic stainless steels hardened by dispersed particles of yttrium, titanium or aluminum oxides (oxide dispersion strengthened (ODS) [1–9]), which, as opposed to carbides, nitrides and intermetallic, do not dissolve when heated to 1400 K. ODS steels are usually produced by a complex technology including mechanical alloying [3]. They have a large resistance to radiation swelling (e.g., $\Delta V/V < 0.1\%$ under irradiation with 4-MeV Ni ions up to 150 dpa [8]) and high-temperature creep. However, it is still not clear how particular regimes of mechanical alloying influence the structure and properties of ODS steels, radiation defects and structure-phase transformations in these steels. The effect of neutron irradiation on degradation of their plasticity characteristics has not been explained either. This paper deals with these issues.

2. Materials

The subjects of study were ODS steels types K2, K5 and K7 (China) [3]. The chemical compositions of the steels are given in Table 1. For comparison sake, a model Fe–13Cr ferritic alloy, ferritic–martensitic (13Cr–2Mo–Nb–V–B) and austenitic (16Cr–15Ni–3Mo–Ti–V) reactor steels were analyzed. The production technology of the ODS steels included the following steps: mechanical alloying of powders with different grain sizes (Fe, 13.9 μm; Cr, 61 μm; Mo, 3.7 μm; Cr–Fe–Ti, 35.6 μm; $Y_2O_3 < 30$ nm) in a ball mill under an argon atmosphere; degassing of the powders at 723 K; hot pressing at 1373 K. The final treatment consisted of annealing at 1373 K (1 h) and cooling in air. The sintered samples prepared by the aforementioned technology were free of pores.

* Corresponding author. Tel.: +7-3432 74 44 94; fax: +7-3432 74 00 03.
E-mail address: bng@imp.uran.ru (B.N. Goshchitskii).

0022-3115/02/$ - see front matter
PII: S0022-3115(02)01047-4

Table 1
Composition of the steels studied (wt%)

Steels	Cr	Ti	Mo	O	N	C	Y_2O_3	W	Al	Ni	Mn	Nb	V
K_2	13.1	2.2	1.4	0.54	0.16	0.02	0.38	–					
K_5	13.5	1.3	0.6	0.27	0.02	0.011	0.39	–	0.17				
K_7	13.4	1.1	0.2	0.24	0.02	0.007	0.39	2.1	0.16				
13Cr–2Mo–Nb–V–B	12.3	–	1.4	–	–	0.13	–	–	–	0.35	0.4	0.4	0.2
16Cr–15Ni–3Mo–Ti–V	16.2	0.4	2.2	–	0.01	0.06	–	–	–	14.3	1.6	–	0.1
Fe–13Cr	12.8	–	–	0.01	0.01	0.01	–	–	–	–	–	–	–

3. Results and discussion

3.1. The effect of mechanical alloying conditions on the structure and mechanical properties

The K2, K5 and K7 ODS steels differed both in their composition and the method of mechanical alloying. The starting powder for the K2 steel was ground in a ball mill for 36 h. The mass ratio of the balls and the powder was 10:1. An average speed of the balls was 110 rpm. The starting powders for the K5 and K7 steels were ground for a longer time (48 h). The mass ratio of the balls and the powder was 15:1, while the balls rotated at an average speed of 150 rpm. The last treatment led to more complete grinding and deformation dissolution of yttrium oxides having an average initial size of ~30 nm. During sintering of the powders and the final thermal treatment, significantly more ultrafine (nanosized) complex oxides Y_2O_3–TiO_2(Y_2TiO_5) [3,4] were precipitated in the ODS steels. An average diameter d and the concentration n of dispersed oxides were determined from an electron microscopic dark-field image [4]. In the K2, K5 and K7 steels, an average sizes of the particles was 3, 2.5 and 3.3 nm at a concentration of 0.4, 2.0 and 1.6×10^{17} cm^{-3}, which corresponded to the volume content of 0.06%, 0.16% and 0.30%, respectively. Dispersed oxide particles ~2–3 nm in size did not dissolve during heating. They pinned dislocations, grain and subgrain boundaries. As a result, an elongated subgrain structure was preserved in the K5 and K7 ODS steels even when the samples were heated to 1373 K or higher [4]. At 293 and 923 K the yield strength $\sigma_{0.2}$ and the ultimate strength σ_B of the K5 and K7 ODS steels were higher than those of K2 having a lower concentration of dispersed oxides. The yield strength of the K5 steel at 293 K, in particular, was nearly 350 MPa higher than $\sigma_{0.2}$ of the K2 steel. The strength properties of the K5 steel annealed at 1373 K ($\sigma_{0.2} = 1272$ MPa; $\sigma_B = 1360$ MPa) were several times better than the corresponding properties of the Fe–13Cr ferritic alloy ($\sigma_{0.2} = 128$ MPa, $\sigma_B = 340$ MPa), while plasticity remained at quite a high level (the specific elongation $\delta = 14.8\%$).

Higher strength characteristics of the K5 and K7 ODS steels (as compared to K2) were preserved during long-term high-temperature tests at 923 and 973 K [4]. A dependence of the creep rate on the applied load for the K2, K5 and K7 ODS steels is shown in logarithmic coordinates in Fig. 1. The creep rate decreases with growing number of dispersed particles of special oxides ($\dot{\varepsilon}$ is a minimum for the K7 steel containing 0.30% particles, and a maximum for the K2 steel containing 0.06% dispersed oxides). The K5 and K7 ODS steels obviously hold advantage in the creep resistance over the common 16Cr–15Ni–3Mo–Ti–V and 13Cr–2Mo–Nb–V–B reactor steels (see Fig. 1) under all loads (150–450 MPa) and temperatures (923–973 K). During a creep, the size of Y_2TiO_5 oxide particles increases a little. However they remain highly dispersed (3–4 nm) [4] and, consequently, determine better strength characteristics.

Properties of ODS steels with 0.38 wt% Y_2O_3 cannot be improved by a standard method of high-temperature powder sintering (without additional mechanical alloying under optimal conditions), since in this case coarse starting oxides ~30 nm in size do not dissolve and, consequently, strengthening ultrafine oxides ~2–3 nm in size do not precipitate during the later treatment. Therefore a proper regime of mechanical alloying is very important in the manufacture of high-strength ODS steels.

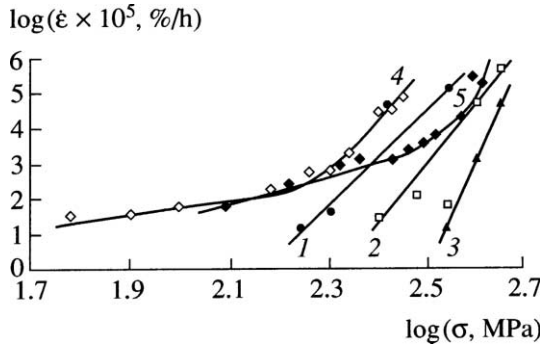

Fig. 1. Dependence of the creep rate $\dot{\varepsilon}$ on the applied stress σ at 650 °C for K2 (1), K5 (2) and K7 (3) ODS steels and common reactor bcc 13Cr–2Mo–Nb–V–B (4) and fcc 16Cr–15Ni–3Mo–Ti–V (5) steels.

3.2. Irradiation at 77, 340 and 683 K

The samples were irradiated with fast neutrons of a fission spectrum in the core of an IVV-2M nuclear reactor at 77 and 340 K and, for comparison, with 5-MeV electrons at 80 K.

Resistivity values of the K5 and Fe–13Cr steels versus the neutron fluence F at an irradiation temperature of 77 K are shown in Fig. 2. When $T_{irr} = 77$ K, resistivity rises mostly thanks to clusters formed in displacement cascades. It should be noted that K5 and Fe–13Cr have similar $\Delta\rho/\rho_0(F)$ dependences ($\Delta\rho$ being an electroresistivity increment after irradiation and ρ_0 the initial value of electroresistivity before irradiation), i.e. when the ODS steels are exposed to neutron irradiation at 77 K, their microstructure does not affect the process of radiation damage.

The change in resistivity of the Fe–13Cr and K5 samples following isochronal annealing after electron irradiation at 80 K is shown in Fig. 3(a) and (b). The electron fluence was $F = 10^{22}$ m^{-2} which, by our estimates, corresponded to $\sim 10^{-4}$ dpa. The concentration of Frenkel pairs, which was calculated from the increment in resistivity under the given fluence, was $\sim 2 \times 10^{-5}$, which is five times less than the experimental value of 10^4 dpa. This fact may be explained by a recombination of adjacent pairs at a 80 K. As is seen from Fig. 3, electroresistivity of both samples changes similarly up to 250 K. This means that interstitial atoms do not interact with impurity atoms which, as distinct from Fe–13Cr, are present in the K5 steel, or they are absent in the solid solution. At a temperature above 250 K electroresistivity of both samples drops below the initial values, a fact which is connected with processes of the short-range ordering. Migration of vacancies in the Fe–13Cr alloy begins at 220 K [10]. In our case an abrupt drop in electroresistivity of the Fe–13Cr alloy was observed at ~350 K (Fig. 3(b)). Earlier we showed that 'vacancy – interstitial atom' complexes (oxygen, nitrogen) dissociated at 350 K [11]. Electroresistivity of the K5 steel decreased to a much smaller extent than electroresistivity of the Fe–13Cr steel (Fig. 3(a)). This is probably due to the fact that the diffusion path of vacancies in K5 is shorter than in Fe–13Cr, because the concentration of vacancy sinks in K5 is much larger. Therefore, given one and the same initial concentration of vacancies, the ordering processes in K5 proceed at a slower rate.

Resistivity exhibits a similar behavior in samples under neutron irradiation (Fig. 4 (a) and (b)). The annealing spectrum of defects (Fig. 4(b)) has a broad peak at 150–170 K, which is connected with migration of interstitial atoms. Oppositely to electron irradiation, no splitting is present to separate peaks since the distance between interstitial atoms and vacancies increases

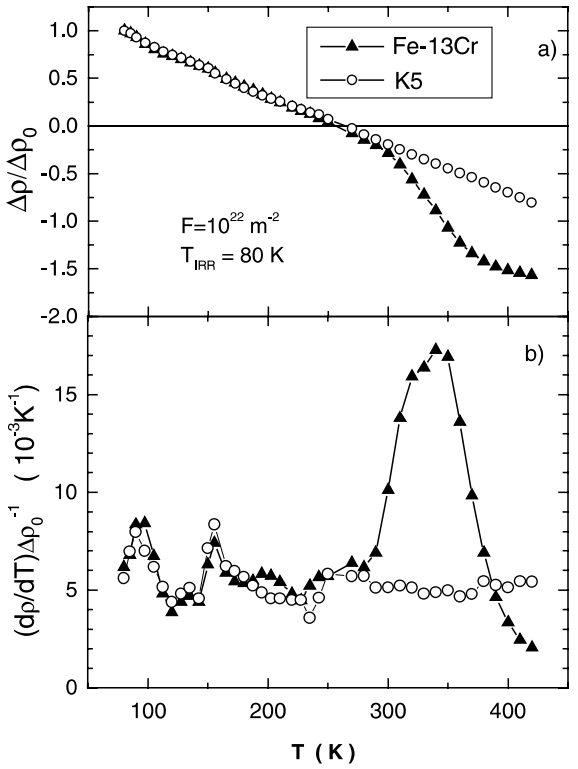

Fig. 3. Integral (a) and differential (b) changes of electroresistivity during isochronal annealing after electron irradiation ($\Delta\rho_0$ being an electroresistivity increment after irradiation and $\Delta\rho$ a change of the current).

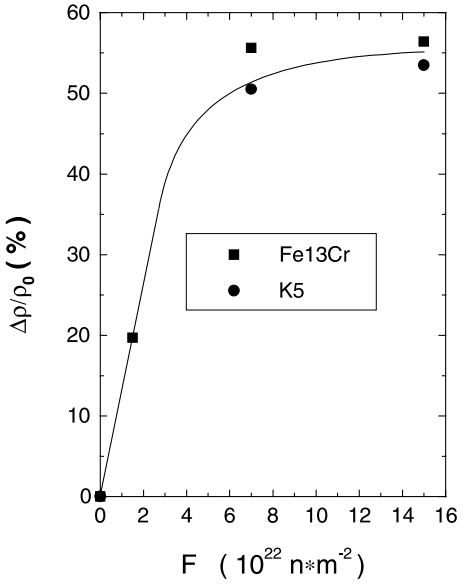

Fig. 2. Relative change of electroresistivity of the samples under a low temperature (77 K) neutron irradiation ($\Delta\rho$ being an electroresistivity increment after irradiation and ρ_0 the initial value of electroresistivity before irradiation).

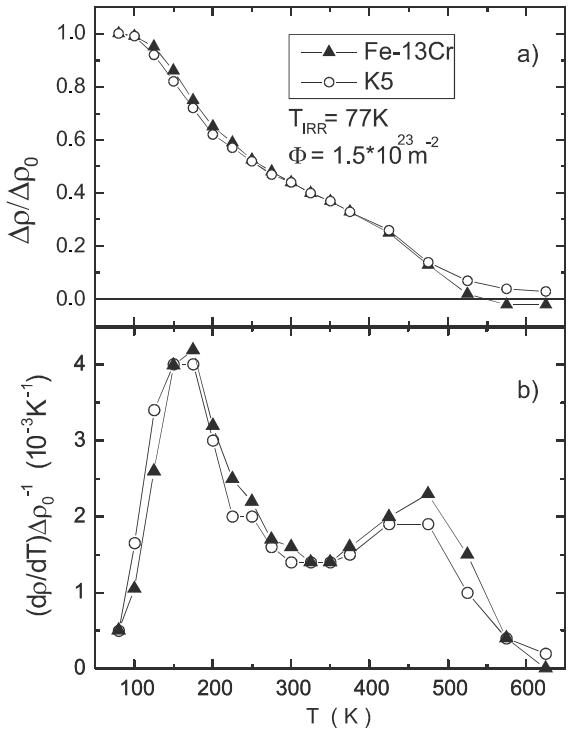

Fig. 4. Integral (a) and differential (b) changes of electroresistivity during isochronal annealing after neutron irradiation.

considerably. A weakly pronounced peak can be seen near 220 K (see Fig. 4(b)), which arises from migration of vacancies. A clearly defined stage of annealing is also observed in the region of 470 K. Earlier it was shown [12] that the peak at 470 K is connected with dissociation of vacancy clusters (in this case, vacancy clusters are formed in displacement cascades). Oppositely to electron irradiation, here $\Delta\rho/\rho_0 \approx 50\%$ and the influence of ordering processes is very weak: $\Delta\rho/\rho_0 \approx 2\%$. However, they show themselves in this case too (the amplitude of the peak at 470 K in the Fe–13Cr alloy is greater than in K5). Therefore the microstructure of the ODS steels is also important at the stage of free-vacancy annealing under neutron irradiation.

The situations differ at an irradiation temperature of 340 and 77 K. At 340 K vacancies and interstitial atoms are mobile and migrate to sinks. Naturally, vacancy clusters are stable at this temperature. The variation of electroresistivity of alloys annealed under isochronal conditions after neutron irradiation at 340 K is shown in Fig. 5. The processes of short-range ordering at this temperature are caused by a radiation-enhanced diffusion. In this case the influence of the infrastructure of ODS steels is apparent too: electroresistivity of ODS steels decreases to a lesser extent than electroresistivity of Fe–13Cr (see Fig. 5). When the samples were annealed under isochronal conditions, a further drop of electro-

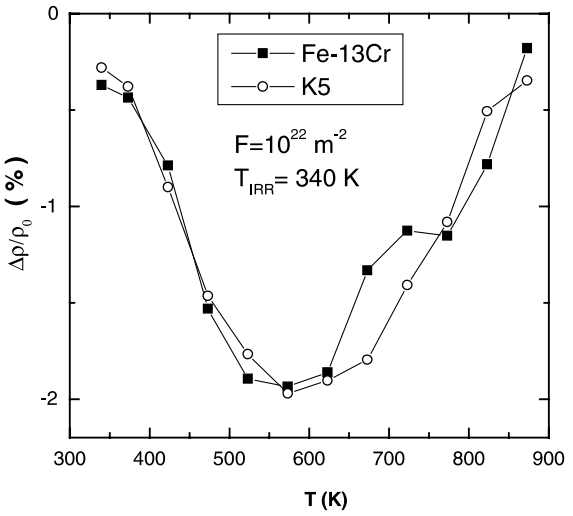

Fig. 5. Variation of relative electroresistivity during isochronal annealing of the samples irradiated with neutrons at 340 K.

resistivity caused by short-range ordering processes was observed in the region of 470 K. The drop was related to dissociation of vacancy clusters and migration of released vacancies. At a temperature above 640 K the effect of thermal diffusion becomes apparent and electroresistivity increases thanks to the decomposition of the solid solution and precipitation of the α'-phase. Table 2 presents experimental values of the tensile properties of the K5 and Fe–13Cr steels after neutron irradiation at 77 K. From Table 2 it is seen that the steels exposed to neutron irradiation at 77 K were hardened thanks to the formation of radiation-defect clusters in displacement cascades. The Fe–13Cr alloy and the ODS steel underwent a marked and complete ($\delta = 0$) embrittlement respectively. It should be noted that an increase in the yield strength of the Fe–13Cr alloy ($\Delta\sigma_{0.2} = 269$ at $F = 1.5 \times 10^{22}$ m^{-2} and $\Delta\sigma_{0.2} = 337$ at $F = 15 \times 10^{22}$ m^{-2}) correlates well with the $(\Delta\rho/\rho_0)^{1/2}$ value rather than with the $(F)^{1/2}$ value (Fig. 2). In other words, when the neutron fluence increases, the concentration of radiation defects comes to saturation, as was shown above. The increment in the ultimate hardening ($\Delta\sigma_{0.2} \sim 340$ MPa) caused by displacement cascades is independent of the test temperatures (77 and 293 K, see Table 2).

An interesting effect was observed when annealing the irradiated samples: the degree of hardening of both samples increased progressively, while the Fe–13Cr alloy got more brittle and brittleness of the K5 steel decreased a little ($\delta = 0.5\%$). As was shown in the foregoing, interstitial atoms and vacancies are annealed in the irradiated samples at 298 K. The short-range ordering and formation of dislocation loops takes place during migration. In this case vacancy clusters and 'vacancy–interstitial atom' complexes are stable. It is probably the

Table 2
Tensile properties of the Fe–13Cr and K5 steels after neutron irradiation

Steels treatment	$F \times 10^{22}$ (n/m^2)	$\sigma_{0.2}$ (MPa)	σ_B (MPa)	δ_u (%)	δ (%)
Fe–13Cr. Test 293 K	0	128	340	–	28
Fe–13Cr. Test 77 K	0	766	846	–	20
Fe–13Cr. Irradiation 77 K. Test 77 K	1.5	1035	1035	0	7.9
	15	1103	1103	0	4.7
Fe–13Cr. Irradiation 77 K + 298 K (24 h). Test 77 K	I5	1179	1179	0	1.8
Fe–13Cr. Irradiation 77 K + 473 K (24 h). Test 77 K	15	1215	1215	0	1.5
Fe–13Cr. Irradiation 77 K. Test 293 K	15	470	480	7.2	14.4
K5–0DS. Irradiation 77 K. Test 77 K	1.5	1795	1795	0	0
K5–0DS. Irradiation 77 K + 298 K (24 h). Test 77 K	1.5	1835	1890	0.5	0.5
K5–0DS. Irradiation 77 K. Test 298 K	1.5	1505	1546	0.7	0.7

short-range ordering and appearance of dislocation loops that causes hardening of the samples. When the Fe–13Cr alloy was annealed at 473 K, hardening and brittleness of the alloy increased still more. It should be noted that hardening depends on the radiation-induced structural phase changes in the ferritic matrix rather than on the segregation of impurities. As was shown above, defect complexes and clusters disintegrate at this temperature, leading, probably, to elimination of hardening. However, dissociation of vacancy clusters is accompanied by appearance of freely migrating vacancies. It is not improbable that the latter process is followed by formation of an ultrafine α'-phase, which causes further hardening. If this assumption is true, particles of the ultrafine α'-phase harden the alloy to a greater extent than displacement cascades.

The K2 steel was also exposed to a fast-neutron fluence of 4.5×10^{26} m^{-2} ($\sim$20 dpa) at 683 K in a BOR-60 reactor. The tensile strength of neutron-irradiated ODS steel increased insignificantly (the yield stress $\sigma_{0.2}$ and the ultimate strength σ_B of K2 at 293 were 1290 and 1465 MPa, respectively), but its plasticity was impaired (the elongation δ decreased to 1.1%). Neutron irradiation of bcc alloys containing over 12% of ferrite-forming elements Cr, Mo and Ti may lead to precipitation of the α'-phase at 673–748 K [8,9]. Formation of the α'-phase causes strengthening and the so-called 475 °C embrittlement.

Acknowledgements

This work was supported financially by the Russian Foundation for Fundamental Research (Project 01-02-16877) and the State Program of Support to Leading Scientific Schools of Russia (Project 00-15-96581).

References

[1] J.J. Huetj, in: Sintered Metal–Ceramic Composites, Elsevier Science Publishers BV, Amsterdam, 1984, p. 197.
[2] L. Dewilde, J. Gedopt, A. Delbrassine, C. Driesen, B. Kazimierzak, Proceedings of the International Conference of Materials for Nuclear Reactor Core Application, Bristol, 1987, p. 271.
[3] T. Yun, S. Bingquan, P. Qingchun, S. Jiguang. Proceedings of the Material for Advanced Energy Systems and Fission and Fusion Engineering, Southwestern Institute of Physics, Chengdu, China, 1995, p. 110.
[4] V.I. Shalaev, V.V. Sagaradze, T.N. Kochetkova, N.F. Vil'danova, T. Yun, S. Jiguang, Q. Wan, Phys. Met. Metall. 91 (3) (2001) 314.
[5] S. Ukai, M. Harada, H. Okada, et al., J. Nucl. Mater. 204 (1993) 65.
[6] S. Ukai, M. Harada, H. Okada, et al., J. Nucl. Mater. 204 (1993) 74.
[7] A.M. Wilson, M.C. Clayden, J. Standring, Proceedings of the International Conference of Materials for Nuclear Reactor Core Application, Bristol, 1987, p. 25.
[8] K. Asano, Y. Kohno, A. Kohyama, T. Suzuki, H. Kusanagi, J. Nucl. Mater. 155–157 (1988) 928.
[9] D.K. Mukhopadhyay, F.H. Froes, D.S. Gelles, J. Nucl. Mater. 258–263 (1998) 1209.
[10] C. Dimitrov, A. Benkaddour, C. Corbel, P. Moser, Ann. Chim. 16 (1991) 319.
[11] A.L. Nikolaev, V.L. Arbuzov, A.E. Davletshin, J. Phys. Condens. Matter 9 (1997) 4385.
[12] V.L. Arbuzov, A.P. Druzhkov, A.L. Nikolaev, S.M. Klotsman, Rad. Eff. Def. Solids 124 (1992) 409.